

Holographic calculation of the QCD crossover temperature in a magnetic field

Romulo Rougemont,^a Renato Critelli,^a Jorge Noronha^{a,b}

^a*Instituto de Física, Universidade de São Paulo, C.P. 66318, 05315-970, São Paulo, SP, Brazil*

^b*Department of Physics, Columbia University, 538 West 120th Street, New York, NY 10027, USA*

E-mail: romulo@if.usp.br, renato.critelli@usp.br, noronha@if.usp.br

ABSTRACT: Lattice data for the QCD equation of state and the magnetic susceptibility computed near the crossover phase transition (at zero magnetic field) are used to determine the input parameters of a five dimensional Einstein-Maxwell-Dilaton holographic model. Once the model parameters are fixed at zero magnetic field, one can use this holographic construction to study the effects of a magnetic field on the equilibrium and transport properties of the quark-gluon plasma. In this paper we use this model to study the dependence of the crossover temperature with an external magnetic field. Our results for the pressure of the plasma and the crossover temperature are in quantitative agreement with current lattice data for values of the magnetic field $0 < eB < 0.3 \text{ GeV}^2$, which is the relevant range for ultrarelativistic heavy ion collision applications.

KEYWORDS: Holography, thermodynamics, magnetic field, equation of state, magnetic susceptibility, crossover transition.

Contents

1	Introduction	1
2	The holographic model	4
2.1	Ultraviolet expansions	5
2.2	Infrared expansions	6
2.3	Coordinate transformations and thermodynamical observables	8
2.4	Fixing the Maxwell-Dilaton gauge coupling using lattice data for the magnetic susceptibility at zero magnetic field	10
3	Holographic QCD thermodynamics at nonzero magnetic field	14
4	Concluding remarks and perspectives	17

1 Introduction

Recent relativistic heavy ion collision experiments [1–4] have produced a strongly coupled quark-gluon plasma (QGP) [5] whose physical properties are currently under intense investigation (see [6, 7] for recent reviews). The study of the equilibrium and transport properties of the QGP as functions of parameters such as the temperature T , chemical potential(s), and (electro)magnetic fields are of great relevance for the characterization and understanding of this new state of QCD matter. In particular, very strong magnetic fields of $\mathcal{O}(0.1\text{--}0.3\text{ GeV}^2)$ are expected to be created in the early stages of noncentral relativistic heavy ion collisions [8–13]¹ and even larger magnetic fields may have been produced in the early stages of the Universe [15, 16] (see, for instance, Fig. 10 in [17]). Also, strong magnetic fields are present in very dense neutron stars known as magnetars [18]. Therefore, the study of the effects of strong magnetic fields on the QGP has sparked a large amount of interest in the community in recent years [19–46] (for extensive reviews and other references, see for instance, [47–50]).

Since the properties of a strongly coupled QGP cannot be reliably studied using perturbative techniques one has to resort to nonperturbative approaches that are valid at strong coupling. Interestingly enough, contrary to what happens in the case of a nonzero baryon chemical potential where the sign problem of the fermion determinant prevents the application of Monte Carlo importance sampling method in lattice simulations (for a review

¹It is not clear at the moment if the electromagnetic fields present in the early stages of heavy ion collisions remain strong enough to directly affect equilibrium and transport properties of the plasma produced at later stages. See for instance [14] for a recent study of how the QGP’s electric conductivity may actually delay the decay of the magnetic field in the medium.

see [51]), in the case of a nonzero magnetic field (at vanishing baryon chemical potential) standard lattice techniques may be employed to study the equilibrium properties of QCD in the (T, B) -plane, see for instance, [17, 52, 53].

Another nonperturbative method that is suited to study strongly coupled non-Abelian gauge theories is the holographic anti-de Sitter/conformal field theory (AdS/CFT) correspondence (also known as the gauge/gravity duality) [54–56]. The correspondence has been employed to obtain useful insight into the properties of strongly coupled gauge theory plasmas such as the strongly coupled QGP, as recently reviewed in [57, 58]. A very attractive feature of the gauge/gravity duality is that it may be easily employed to compute transport coefficients of strongly coupled non-Abelian gauge theory plasmas (see, for instance, [59–63]), which is a challenging task to perform on the lattice [64].

A top-down holographic dual for $\mathcal{N} = 4$ super Yang-Mills theory (SYM) in the presence of an external constant magnetic field was proposed in [65–67] and calculations for different physical observables in this scenario were carried out, for instance, in [68–71]. However, the QGP formed in heavy ion collisions [6, 7] probes the temperature region within which the QCD plasma is highly nonconformal [72] (when $T \sim 150 - 400$ MeV). Therefore, in order to make contact with realistic heavy ion collision applications, one needs to develop holographic models that are able to capture some of the relevant aspects of the physics of the strongly coupled QGP near the crossover transition [73]. One possible way to accomplish this within holography is to deform the boundary quantum field theory by turning on a dynamical scalar field profile in the bulk whose boundary value sources a relevant gauge invariant operator in the gauge theory. Near the boundary the scalar field profile approaches zero and conformal invariance is recovered in the ultraviolet. In the infrared, however, the holographic dual gauge theory generated by such deformation behaves very differently than a conformal plasma and may be tuned to display some of the properties of QCD in the strong coupling regime.

In this work we construct a nonconformal, anisotropic bottom-up holographic model that is suited for the study of a QCD-like plasma at nonzero magnetic field and vanishing chemical potential(s). Our model is built up on classical nonconformal anisotropic black brane solutions for the Einstein-Maxwell-Dilaton (EMD) model defined with a negative cosmological constant and in the presence of an external, constant magnetic field. This constitutes a sequel to the studies of strongly coupled nonconformal plasmas via black brane solutions initiated in [59, 74] in the case of finite temperature, zero magnetic field, and vanishing chemical potential², which was later extended in [62, 79] (see also [63]) to take into account the presence of a nonzero baryon chemical potential and zero magnetic field³. This type of nonconformal model has been used in the last years to investigate how

²These nonconformal solutions can also be adapted to study the vacuum properties of the gauge theory, as recently discussed in [75]. This was studied in detail earlier in [76–78] in the case of similar bottom-up models at zero and finite temperature concerning pure Yang-Mills theory.

³See also [80] for a bottom-up holographic model at finite temperature, nonzero chemical potential, and zero magnetic field in the Veneziano limit [81].

different observables of phenomenological relevance to the QGP and the physics of heavy ion collisions vary near the QCD crossover transition. In fact, after the original calculations in [59, 74], which included the evaluation of the bulk viscosity at zero baryon chemical potential and zero magnetic field [59], a series of other quantities were computed within this type of holographic model such as the heavy quark free energy [82, 83], the energy loss of highly energetic probes [84–86], the Debye screening mass [75], the electric conductivity [60], a large set of first and second order viscous hydrodynamic transport coefficients [61] and, recently, the spectrum of quasinormal modes near the crossover transition has also been computed within this model [87]. We also mention, in the context of the holographic models developed in [62, 79], as extensions of the original models [59, 74], taking into account the presence of a nonvanishing baryon chemical potential, the calculation of the holographic critical point in the (T, μ_B) -plane [79], and the evaluation of the baryon conductivity and bulk viscosity at finite baryon chemical potential and zero magnetic field [62]. Here we add one more entry to this family of solutions by taking into account the presence of a magnetic field in the nonconformal, QCD-like gauge theory.

Our model is a bottom-up holographic setup in which the dilaton potential and the Maxwell-Dilaton gauge coupling are fixed in order to describe lattice data at zero chemical potential and magnetic field, which should be contrasted with top-down models coming from compactifications of known string theory solutions. Although in bottom-up models the holographic dual is not precisely known due to the fact that these models are constructed using some phenomenological input from QCD, at least part of the physics of the boundary gauge field theory may resemble QCD in the strong coupling limit. Thus, one may regard such constructions as holographic effective theories that are engineered to model some specific aspects of QCD phenomenology. Once the model parameters are fixed, these theories can be used to make predictions about observables that are currently beyond the scope of lattice calculations, such as most of the second order hydrodynamic coefficients [61].

This paper is organized as follows. In Section 2 we describe in detail the construction of our holographic model and how the dilaton potential and the Maxwell-Dilaton gauge coupling can be determined by lattice data for the $(2 + 1)$ -flavor lattice QCD equation of state and magnetic susceptibility at zero magnetic field, respectively. With the holographic model parameters fully specified, we proceed in Section 3 to obtain the holographic equation of state at nonzero magnetic field and present results for the temperature and magnetic field dependence of the entropy density and the pressure. We find that the deconfinement temperature in our holographic model decreases with an increasing magnetic field, as recently observed on the lattice. Moreover, our model results for the pressure and the crossover temperature are in quantitative agreement with current lattice data up to moderately large magnetic fields $eB < 0.3 \text{ GeV}^2$. We finish the paper in Section 4 where we also point out other applications to be pursued in the near future using the anisotropic, nonconformal holographic model developed here.

Throughout this paper we use natural units $c = \hbar = k_B = 1$ and a mostly plus metric

signature.

2 The holographic model

In this section we construct a bottom-up EMD model that may be used to estimate the properties of the strongly coupled QGP in the presence of an external magnetic field. Many of the steps taken here are very similar to those followed in [62, 79] (see also [63]) for the case of zero magnetic field and nonzero chemical potential, which may be also described by an EMD model with a different Ansatz for the bulk fields than what we are going to consider below. More specifically, the difference stems from the fact that the magnetic field makes the five dimensional background geometry anisotropic while a chemical potential can be introduced without breaking rotational invariance.

The action for the EMD model is

$$S = \frac{1}{16\pi G_5} \int_{\mathcal{M}_5} d^5x \sqrt{-g} \left[R - \frac{1}{2}(\partial_\mu \phi)^2 - V(\phi) - \frac{f(\phi)}{4} F_{\mu\nu}^2 \right] + S_{\text{GHY}} + S_{\text{CT}}, \quad (2.1)$$

where S_{GHY} is the Gibbons-Hawking-York action [88, 89] needed to establish a well-posed variational problem with Dirichlet boundary condition for the metric, and S_{CT} is the counterterm action that can be constructed using the holographic renormalization procedure [90–94]. These two boundary terms contribute to the total on-shell action but not to the equations of motion and, since we shall not need to compute the total on-shell action in the present work, we do not need to worry about their explicit form here.

In (2.1), the metric field in the bulk is dual to the stress-energy tensor of the boundary field theory while the dilaton field is introduced in order to dynamically break the conformal symmetry of the gauge theory. On the other hand, the Abelian gauge field in the bulk is employed here to introduce an external magnetic field at the boundary, which we take to be constant and uniform in the \hat{z} -direction. The presence of this constant magnetic field breaks the $SO(3)$ rotational invariance of the gauge theory down to $SO(2)$ rotations around the \hat{z} -axis. This implies that the Ansatz for the bulk metric must be anisotropic. Also, at zero temperature this Ansatz must be invariant under boosts in the (t, z) -plane though this symmetry is not present at nonzero temperature. Based on these remarks, one may propose the following black brane Ansatz for the bulk fields in⁴ (2.1):

$$ds^2 = e^{2a(r)} [-h(r)dt^2 + dz^2] + e^{2c(r)}(dx^2 + dy^2) + \frac{e^{2b(r)}dr^2}{h(r)},$$

$$\phi = \phi(r), \quad A = A_\mu dx^\mu = \mathcal{B}x dy \Rightarrow F = dA = \mathcal{B}dx \wedge dy, \quad (2.2)$$

⁴As we shall discuss soon, \mathcal{B} is one of the two initial conditions controlling the temperature and the external magnetic field at the boundary quantum field theory. The other initial condition corresponds to the value of the dilaton field evaluated at the black brane horizon, ϕ_0 . The set of initial conditions (ϕ_0, \mathcal{B}) is nontrivially related to the thermodynamical pair (T, B) in the gauge theory. In subsections 2.3 and 2.4 we discuss how one can relate \mathcal{B} to the external magnetic field at the boundary gauge theory, B .

where the radial location of the black brane horizon, r_H , is given by the largest root of the equation $h(r_H) = 0$ and in our coordinates the boundary of the asymptotically AdS₅ spacetime is located at $r \rightarrow \infty$. In (2.2) we have already fixed a convenient gauge for the Maxwell field, which in the present case is a prescribed non-dynamical field. Also, for simplicity, we shall adopt units where the asymptotic AdS₅ radius is equal to one.

Using (2.2), the equations of motion obtained from (2.1) may be expressed as follows

$$\phi'' + \left(2a' + 2c' - b' + \frac{h'}{h}\right) \phi' - \frac{e^{2b}}{h} \left(\frac{\partial V(\phi)}{\partial \phi} + \frac{\mathcal{B}^2 e^{-4c}}{2} \frac{\partial f(\phi)}{\partial \phi}\right) = 0, \quad (2.3)$$

$$a'' + \left(\frac{14}{3}c' - b' + \frac{4h'}{3h}\right) a' + \frac{8}{3}a'^2 + \frac{2}{3}c'^2 + \frac{2h'}{3h}c' + \frac{2e^{2b}}{3h}V(\phi) - \frac{1}{6}\phi'^2 = 0, \quad (2.4)$$

$$c'' - \left(\frac{10}{3}a' + b' + \frac{1h'}{3h}\right) c' + \frac{2}{3}c'^2 - \frac{4}{3}a'^2 - \frac{2h'}{3h}a' - \frac{1e^{2b}}{3h}V(\phi) + \frac{1}{3}\phi'^2 = 0, \quad (2.5)$$

$$h'' + (2a' + 2c' - b') h' = 0, \quad (2.6)$$

where the prime denotes a derivative with respect to the radial direction. Using these equations of motions one can also derive a useful constraint

$$a'^2 + c'^2 - \frac{1}{4}\phi'^2 + \left(\frac{a'}{2} + c'\right) \frac{h'}{h} + 4a'c' + \frac{e^{2b}}{2h} \left(V(\phi) + \frac{\mathcal{B}^2 e^{-4c}}{2} f(\phi)\right) = 0. \quad (2.7)$$

The equation of motion for the Maxwell field is automatically satisfied by the Ansatz (2.2). Moreover, $b(r)$ has no equation of motion and, thus, it can be freely chosen to take any value due to reparametrization property of the radial coordinate. In the next subsection we specify a subsidiary condition for $b(r)$ that defines a convenient gauge for the metric that will be used in the numerical calculations carried out in the present work.

2.1 Ultraviolet expansions

For the calculation of physical observables in the gauge theory one needs to obtain the near-boundary, far from the horizon expansions for the bulk fields $a(r)$, $c(r)$, $h(r)$, and $\phi(r)$. In the present work, we use the domain-wall gauge defined by the subsidiary condition $b(r) = 0$. At the boundary the dilaton field goes to zero in such a way that $V(\phi(r \rightarrow \infty) \rightarrow 0) = -12$ and $f(0)$ is a finite, positive constant⁵. Also, the metric blackening factor, $h(r)$, must go to a constant at the boundary, which we denote by⁶ $h(r \rightarrow \infty) = h_0^{\text{far}}$.

Moreover, since we are interested in asymptotically AdS₅ solutions to the equations of motion (2.3), (2.4), (2.5), and (2.6) at the boundary one finds $a(r \rightarrow \infty) = c(r \rightarrow \infty)$. In

⁵Note that in (2.1) the Maxwell-Dilaton gauge coupling, $f(\phi)$, plays the role of an inverse effective gauge coupling squared and, therefore, it must correspond to a positive-definite function.

⁶This constant is equal to one in the so-called “standard coordinates” of the domain-wall gauge, which we shall discuss soon. Here we are considering general coordinates where this constant may be different than one. We shall also see later how to relate these two sets of coordinates.

the domain-wall gauge $b(r) = 0$, the leading order near-boundary expression for $a(r)$ (and also $c(r)$) is linear in r [62, 79] such that at lowest order in $\phi(r \rightarrow \infty) \rightarrow 0$ we may consider the following leading order far from the horizon ultraviolet asymptotics

$$V(\phi) \approx -12, \quad f(\phi) \approx f(0), \quad h(r) \approx h_0^{\text{far}}, \quad a(r) \approx a_0^{\text{far}} + a_{-1}^{\text{far}} r, \quad c(r) \approx c_0^{\text{far}} + c_{-1}^{\text{far}} r, \quad (2.8)$$

where $a_{-1}^{\text{far}} = c_{-1}^{\text{far}}$, as discussed above. Indeed, by substituting (2.8) into the equations of motion and taking the asymptotic limit of large r (where the ultraviolet expansions hold), one concludes that

$$a_{-1}^{\text{far}} = c_{-1}^{\text{far}} = \frac{1}{\sqrt{h_0^{\text{far}}}}. \quad (2.9)$$

In order to obtain the next to leading order term for $h(r)$ and also the first terms for $\phi(r)$ in the ultraviolet expansions for the bulk fields, we consider the first backreaction of the near-boundary fields expressed in (2.8) and (2.9) on the equations of motion⁷. In fact, we first consider the next to leading order near-boundary expansion for the dilaton potential

$$V(\phi) \approx -12 + \frac{m^2}{2} \phi^2, \quad m^2 = -\nu \Delta, \quad (2.10)$$

where Δ is the ultraviolet scaling dimension of the gauge invariant operator dual to the bulk dilaton field and we defined $\nu = d - \Delta$, where $d = 4$ is the dimension of the boundary. We shall see in Section 2.4 that a reasonable description of lattice data can be achieved by taking $\Delta \approx 3$ ($\nu \approx 1$). One can now show that the far from horizon ultraviolet asymptotics for the bulk fields may be written as

$$\begin{aligned} a(r) &\approx \alpha(r) + \dots, \\ c(r) &\approx \alpha(r) + (c_0^{\text{far}} - a_0^{\text{far}}) + \dots, \\ h(r) &\approx h_0^{\text{far}} + h_4^{\text{far}} e^{-4\alpha(r)} + \dots, \\ \phi(r) &\approx \phi_A e^{-\nu\alpha(r)} + \phi_B e^{-\Delta\alpha(r)} + \dots, \end{aligned} \quad (2.11)$$

where we defined $\alpha(r) = a_0^{\text{far}} + r/\sqrt{h_0^{\text{far}}}$ while \dots denotes subleading terms. We note that the ultraviolet asymptotics (2.11) are in agreement with our numerical solutions. By comparing these numerical solutions to (2.11) one can determine the ultraviolet coefficients a_0^{far} , c_0^{far} , h_0^{far} and ϕ_A , which are needed to compute the thermodynamical observables in subsections 2.3 and 2.4.

2.2 Infrared expansions

Now we consider the infrared, near-horizon expansions for the bulk fields $a(r)$, $c(r)$, $h(r)$, and $\phi(r)$. Near the horizon all the bulk fields in (2.2) are assumed to be smooth and

⁷This procedure may be repeated to obtain all the other subleading terms in the ultraviolet expansions. However, we only need the first few terms in these expansions to compute the thermodynamical observables.

we may consider the Taylor expansions

$$X(r) = \sum_{n=0}^{\infty} X_n (r - r_H)^n, \quad (2.12)$$

where $X = \{a, c, h, \phi\}$.

In order to numerically solve the equations of motion (2.3), (2.4), (2.5), and (2.6) we need to specify the boundary conditions $X(r_{\text{start}})$ and $X'(r_{\text{start}})$, where r_{start} is a value of the radial coordinate that is slightly above the horizon⁸. In this paper we work with the Taylor expansions up to second order, which are sufficient to perform the numerical integrations if r_{start} is close enough to r_H . Therefore, we must determine 12 Taylor coefficients in order to specify $X(r_{\text{start}})$ and $X'(r_{\text{start}})$ at second order. One of these 12 coefficients, namely, ϕ_0 , is one of the two initial conditions of the problem⁹. Four of these 12 coefficients, namely, a_0 , c_0 , h_0 , and h_1 and also the radial location of the black hole horizon, r_H , may be fixed by rescaling the bulk coordinates while taking into account also the fact that $h(r)$ vanishes at the horizon. For definiteness, we adopt here numerical coordinates fixed in such a way that

$$r_H = 0; \quad a_0 = c_0 = h_0 = 0, \quad h_1 = 1. \quad (2.13)$$

Note that $r_H = 0$ may be obtained by rescaling the radial coordinate while $h_0 = 0$ comes from the fact that $h(r)$ has a simple zero at the horizon. Also, $h_1 = 1$ may be obtained by rescaling t while $a_0 = 0$ may be arranged by rescaling (t, z) by a common factor. Similarly, $c_0 = 0$ may be arranged by rescaling (x, y) by a common factor. After this, the remaining 7 coefficients in the near-horizon Taylor expansions for the bulk fields can be fixed on-shell as functions of the initial conditions (ϕ_0, \mathcal{B}) by substituting the second order Taylor expansions into the equations of motion and setting to zero each power of r_{start} in the resulting algebraic equations¹⁰.

With $X(r_{\text{start}})$ and $X'(r_{\text{start}})$ determined as discussed above, the equations of motion are numerically integrated from r_{start} near the horizon up to some numerical ultraviolet cutoff r_{max} near the boundary. We used $r_{\text{start}} = 10^{-8}$ and $r_{\text{max}} = 10$ to numerically solve the equations of motion. It is important to remark, however, that even before reaching $r_{\text{conformal}} = 2$ the numerical backgrounds we considered in the present work have already reached the ultraviolet fixed point corresponding to the AdS₅ geometry. This fact is used in Section 2.3 to reliably obtain the ultraviolet coefficients in (2.11) and it will be also employed in Section 2.4 to properly compute the holographic magnetic susceptibility numerically.

⁸The horizon is a singular point of the equations of motion and, thus, we need to initialize the numerical integrations slightly above it.

⁹As discussed before, the other initial condition is \mathcal{B} .

¹⁰In practice, we set to zero the following 7 terms: $\mathcal{O}(r_{\text{start}}^0)$, $\mathcal{O}(r_{\text{start}}^1)$, and $\mathcal{O}(r_{\text{start}}^2)$ in (2.6), $\mathcal{O}(r_{\text{start}}^{-1})$ in (2.7), $\mathcal{O}(r_{\text{start}}^{-1})$ and $\mathcal{O}(r_{\text{start}}^0)$ in (2.3), and $\mathcal{O}(r_{\text{start}}^0)$ in (2.4).

2.3 Coordinate transformations and thermodynamical observables

Let us now introduce the so-called “standard coordinates” of the domain-wall metric gauge, $\tilde{b}(\tilde{r}) = 0$, where variables with \sim refer to quantities evaluated in these standard coordinates where the background reads

$$d\tilde{s}^2 = e^{2\tilde{a}(\tilde{r})} \left[-\tilde{h}(\tilde{r})d\tilde{t}^2 + d\tilde{z}^2 \right] + e^{2\tilde{c}(\tilde{r})}(d\tilde{x}^2 + d\tilde{y}^2) + \frac{d\tilde{r}^2}{\tilde{h}(\tilde{r})},$$

$$\tilde{\phi} = \tilde{\phi}(\tilde{r}), \quad \tilde{A} = \tilde{A}_\mu d\tilde{x}^\mu = \hat{B}\tilde{x}d\tilde{y} \Rightarrow \tilde{F} = d\tilde{A} = \hat{B}d\tilde{x} \wedge d\tilde{y}, \quad (2.14)$$

and the boundary is at $\tilde{r} \rightarrow \infty$ while the horizon is at $\tilde{r} = \tilde{r}_H$. The “hat” in \hat{B} accounts for the fact that this is the magnetic field written in terms of (5-dimensional) black brane quantities while B (or, more precisely, eB) corresponds to the boundary magnetic field in physical units (MeV^2), as we shall discuss in subsection 2.4. In the standard coordinates, the ultraviolet asymptotics for the bulk fields are given by [62, 79] (see also [63])

$$\begin{aligned} \tilde{a}(\tilde{r}) &\approx \tilde{r} + \dots, \\ \tilde{c}(\tilde{r}) &\approx \tilde{r} + \dots, \\ \tilde{h}(\tilde{r}) &\approx 1 + \dots, \\ \tilde{\phi}(\tilde{r}) &\approx e^{-\nu\tilde{r}} + \dots. \end{aligned} \quad (2.15)$$

The standard coordinates (in which $h(r)$ goes to one at the boundary) are the coordinates where we obtain standard holographic formulas for the gauge theory’s physical observables such as the temperature and the entropy density. However, in order to obtain numerical solutions for the bulk fields one needs to give numerical values for all the infrared near-horizon Taylor expansion coefficients, which in turn requires rescaling these standard coordinates, as discussed in the previous subsection. The numerical solutions are obtained in the *numerical coordinates* described by the Ansatz (2.2) with the ultraviolet asymptotics (2.11), while standard holographic formulas for physical observables are obtained in the standard coordinates described by the background (2.14) with the ultraviolet asymptotics (2.15). Therefore, one can relate these two sets of coordinates by equating $\tilde{\phi}(\tilde{r}) = \phi(r)$, $d\tilde{s}^2 = ds^2$ and $\hat{B}d\tilde{x} \wedge d\tilde{y} = \mathcal{B}dx \wedge dy$ and this leads to the following relations¹¹ (by comparing

¹¹As mentioned in [79] if $\phi_A < 0$ one must replace $\phi_A \mapsto |\phi_A|$ in these relations.

the near-boundary asymptotics (2.11) and (2.15) for $r \rightarrow \infty$)

$$\begin{aligned}
\tilde{r} &= \frac{r}{\sqrt{h_0^{\text{far}}}} + a_0^{\text{far}} - \ln\left(\phi_A^{1/\nu}\right), \\
\tilde{t} &= \phi_A^{1/\nu} \sqrt{h_0^{\text{far}}} t, \\
\tilde{x} &= \phi_A^{1/\nu} e^{c_0^{\text{far}} - a_0^{\text{far}}} x, \\
\tilde{y} &= \phi_A^{1/\nu} e^{c_0^{\text{far}} - a_0^{\text{far}}} y, \\
\tilde{z} &= \phi_A^{1/\nu} z; \\
\tilde{a}(\tilde{r}) &= a(r) - \ln\left(\phi_A^{1/\nu}\right), \\
\tilde{c}(\tilde{r}) &= c(r) - (c_0^{\text{far}} - a_0^{\text{far}}) - \ln\left(\phi_A^{1/\nu}\right), \\
\tilde{h}(\tilde{r}) &= \frac{h(r)}{h_0^{\text{far}}}, \\
\tilde{\phi}(\tilde{r}) &= \phi(r); \\
\hat{B} &= \frac{e^{2(a_0^{\text{far}} - c_0^{\text{far}})}}{\phi_A^{2/\nu}} \mathcal{B}.
\end{aligned} \tag{2.16}$$

The temperature of the plasma is given by the black brane horizon's Hawking temperature

$$\hat{T} = \frac{\sqrt{-\tilde{g}'_{\tilde{t}\tilde{t}} \tilde{g}^{\tilde{r}\tilde{r}}'}}{4\pi} \Big|_{\tilde{r}=\tilde{r}_H} = \frac{e^{\tilde{a}(\tilde{r}_H)}}{4\pi} |\tilde{h}'(\tilde{r}_H)| = \frac{1}{4\pi \phi_A^{1/\nu} \sqrt{h_0^{\text{far}}}}, \tag{2.17}$$

while the entropy density is obtained via the Bekenstein-Hawking's relation [95, 96]

$$\hat{s} = \frac{S}{V} = \frac{A_H/4G_5}{V} = \frac{\int_{\text{horizon}} d^3\tilde{x} \sqrt{\tilde{g}(\tilde{r}=\tilde{r}_H, \tilde{t} \text{ fixed})}}{4G_5 V} = \frac{2\pi e^{\tilde{a}(\tilde{r}_H) + 2\tilde{c}(\tilde{r}_H)}}{\kappa^2} = \frac{2\pi e^{2(a_0^{\text{far}} - c_0^{\text{far}})}}{\kappa^2 \phi_A^{3/\nu}}, \tag{2.18}$$

where we defined $\kappa^2 = 8\pi G_5$ and used (2.12), (2.13), and (2.16).

One can see from (2.16), (2.17), and (2.18) that the only ultraviolet coefficients in the numerical coordinates which we need to fix by fitting the numerical solutions with (2.11) are a_0^{far} , c_0^{far} , h_0^{far} , and ϕ_A . The numerical solutions for $h(r)$ converge quickly to their asymptotic values at large r and we may reliably set $h_0^{\text{far}} = h(r_{\text{conformal}})$. With h_0^{far} fixed in this way, we may fix a_0^{far} , c_0^{far} , and ϕ_A , respectively, by employing the fitting functions $a(r) = a_0^{\text{far}} + r/\sqrt{h_0^{\text{far}}}$, $c(r) = c_0^{\text{far}} + r/\sqrt{h_0^{\text{far}}}$, and $\phi(r) = \phi_A e^{-\nu a(r)}$ in the interval $r \in [r_{\text{conformal}} - 1, r_{\text{conformal}}]$. We were able to obtain good fits for the near-boundary behavior of the numerical solutions using this fitting scheme.

Also, it is important to remark that there is an upper bound on the initial condition \mathcal{B} for a given value of the initial condition for the dilaton ϕ_0 . In fact, for values of \mathcal{B} above

this bound, all the numerical backgrounds we generated failed to be asymptotically AdS₅. Such a bound, which we denote by $\mathcal{B} \leq \mathcal{B}_{\max}(\phi_0)$, may be numerically constructed by interpolating a list with pairs of points $\{(\phi_0^i, \mathcal{B}_{\max}^i), i = 1, 2, 3, \dots\}$ and the corresponding result is presented in Fig. 1.

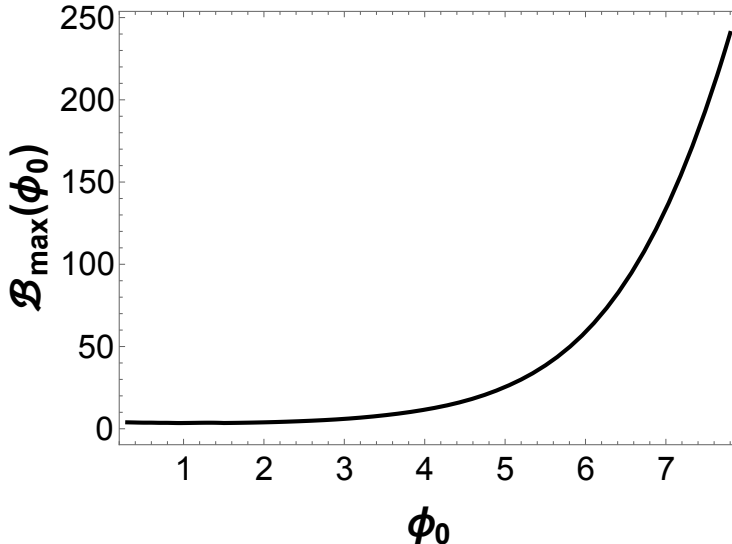


Figure 1: The curve corresponds to the upper bound for the initial condition \mathcal{B} , as a function of the initial condition for the dilaton ϕ_0 , below which the solutions of the equations of motion are asymptotically AdS₅.

In the next section we explain how one can express the thermodynamical quantities \hat{B} , \hat{T} , and \hat{s} in physical units¹² using the lattice data for the equation of state and the magnetic susceptibility at zero magnetic field.

2.4 Fixing the Maxwell-Dilaton gauge coupling using lattice data for the magnetic susceptibility at zero magnetic field

Ref. [61] discussed in detail how to fix the dilaton potential, $V(\phi)$, and the gravitational constant, κ^2 , using the recent lattice data [72] for the QCD equation of state with (2 + 1)-flavors. We refer the reader to that paper for the details about this procedure. The results are

$$V(\phi) = -12 \cosh(0.606 \phi) + 0.703 \phi^2 - 0.1 \phi^4 + 0.0034 \phi^6, \quad \kappa^2 = 8\pi G_5 = 12.5. \quad (2.19)$$

Note that, from the dilaton potential specified above, one obtains the dilaton mass $m^2 \approx -3$, as anticipated in Section 2.1.

¹²Note from (2.16), (2.17), and (2.18) that \hat{B} , \hat{T} , and \hat{s} are proportional to $\phi_A^{-2/\nu}$, $\phi_A^{-1/\nu}$ and $\phi_A^{-3/\nu}$, respectively. Correspondingly, their counterparts in physical units (without the “hat”) are given in MeV², MeV, and MeV³, respectively. This is related to the fact that the leading mode for the dilaton field, ϕ_A , corresponds to the insertion of a relevant deformation in the quantum field theory, which is responsible for generating an infrared scale that breaks the conformal invariance of the theory at low energies [62].

In the present paper, we also use the same procedure used in [61] to express the holographically determined thermodynamical observables in physical units, i.e., we find the temperature at which our speed of sound squared, c_s^2 , displays a minimum (at zero magnetic field) and match it to the corresponding lattice QCD result [72]

$$\lambda = \frac{T_{\min. c_s^2}^{\text{lattice}}}{T_{\min. c_s^2}^{\text{BH}}} \approx \frac{143.8 \text{ MeV}}{0.173} \approx 831 \text{ MeV}. \quad (2.20)$$

In what follows, we relate any black hole thermodynamical observable, \hat{X} , with its counterpart in physical units, X , with mass dimension $[\text{MeV}^p]$, by taking $X = \lambda^p \hat{X}$ $[\text{MeV}^p]$. This prescription respects the fact that dimensionless ratios, such as s/T^3 , must give the same result regardless of the units. A comparison between our holographic results for the speed of sound squared, $c_s^2(T, B = 0)$, and the (normalized) pressure, $p(T, B = 0)/T^4$ (at zero magnetic field) and the corresponding lattice QCD results from [72] is shown in Fig. 2. One can see that the holographic model provides a good description of the lattice data in the absence of an external magnetic field, as previously found in [61].

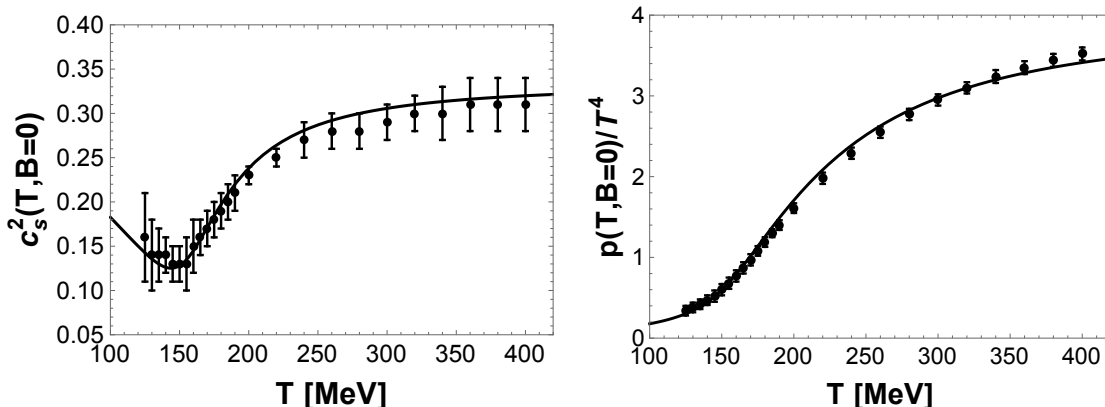


Figure 2: Holographic calculation of the speed of sound squared c_s^2 and the (normalized) pressure p/T^4 . The data points correspond to lattice QCD results from [72] computed at zero magnetic field.

In order to fully determine our holographic model and include the effects from a magnetic field we also need to fix the Maxwell-Dilaton gauge coupling, $f(\phi)$. This can be done using the recent lattice data [52] for the magnetic susceptibility of QCD with $(2+1)$ -flavors evaluated at zero magnetic field. In order to compute the magnetic susceptibility in our holographic model we follow the same general steps discussed in [97]:

- We substitute the Ansatz (2.2) into the action (2.1);
- Next, we calculate the second derivative of the off-shell action with respect to the magnetic field and divide the result by the entire spacetime volume of the boundary;

- In order to obtain the (bare) magnetic susceptibility we plug the on-shell numerical solutions into the expression obtained in the previous step.

Then, following this procedure we find that the bare magnetic susceptibility is¹³

$$\begin{aligned}\chi_{\text{bare}}(T, B) &= -\frac{\partial^2 f_{\text{bare}}}{\partial B^2} = -\frac{1}{V_{\text{bdy}}} \frac{\partial^2 S_{E, \text{bare}}^{\text{on-shell}}[B]}{\partial B^2} = \frac{1}{V_{\text{bdy}}} \frac{\partial^2 S_{\text{bare}}^{\text{on-shell}}[B]}{\partial B^2} \\ &= -\frac{1}{2\kappa^2} \int_{\tilde{r}_H}^{\tilde{r}_{\text{max}}^{\text{fixed}}} d\tilde{r} f(\tilde{\phi}(\tilde{r})) e^{2(\tilde{a}(\tilde{r}) - \tilde{c}(\tilde{r}))} \Big|_{\text{on-shell}},\end{aligned}\tag{2.21}$$

where, formally, one should take the limit $\tilde{r}_{\text{max}}^{\text{fixed}} \rightarrow \infty$. However, in numerical calculations, $\tilde{r}_{\text{max}}^{\text{fixed}}$ must be a fixed ultraviolet cutoff for all the geometries in order to ensure that the ultraviolet divergence in (2.21) is independent of the temperature. Since we are interested here in calculating the magnetic susceptibility at zero magnetic field where $a(r) = c(r)$, one obtains from (2.21)

$$\chi_{\text{bare}}(T, B = 0) = -\frac{1}{2\kappa^2} \int_{\tilde{r}_H}^{\tilde{r}_{\text{max}}^{\text{fixed}}} d\tilde{r} f(\tilde{\phi}(\tilde{r})) \Big|_{\text{on-shell}}.\tag{2.22}$$

In order to regularize (2.22) we follow the same procedure adopted on the lattice [52] and subtract from (2.22) the vacuum contribution at zero temperature. Clearly, this removes the ultraviolet divergences since those are temperature independent. More precisely, we subtract the geometry corresponding to $(T_{\text{small}}, B) \approx (0.005 \text{ MeV}, 0)$, which is generated by the initial conditions $(\phi_0, \mathcal{B}) = (7.8, 0)$; this is the asymptotically AdS₅ geometry with the lowest temperature and zero magnetic field which we could reach in our numerical computations¹⁴. Therefore, we obtain the following holographic formula for the magnetic susceptibility at zero magnetic field (which is valid for any EMD model of the kind considered here)

$$\begin{aligned}\chi(T, B = 0) &= \chi_{\text{bare}}(T, B = 0) - \chi_{\text{bare}}(T_{\text{small}}, B = 0) \\ &= -\frac{1}{2\kappa^2} \left[\left(\int_{\tilde{r}_H}^{\tilde{r}_{\text{max}}^{\text{fixed}}} d\tilde{r} f(\tilde{\phi}(\tilde{r})) \right) \Big|_{T, B=0} - (\text{same}) \Big|_{T_{\text{small}}, B=0} \right]_{\text{on-shell}} \\ &= -\frac{1}{2\kappa^2} \left[\left(\frac{1}{\sqrt{h_0^{\text{far}}}} \int_{r_{\text{start}}}^{r_{\text{max}}^{\text{var}}} dr f(\phi(r)) \right) \Big|_{T, B=0} - (\text{same}) \Big|_{T_{\text{small}}, B=0} \right]_{\text{on-shell}},\end{aligned}\tag{2.23}$$

¹³As mentioned in footnote 7 of [97], the Euclidean action has the opposite sign of the Lorentzian action (2.1).

¹⁴Note that $\phi_0 = 7.8$ corresponds to the local minimum of our dilaton potential (2.19). For $\phi_0 > 7.8$, our dilaton potential becomes non-monotonic and, in practice, we observed that no asymptotically AdS₅ solutions could be produced in this case. Therefore, we took $\phi_0 = 7.8$ as the upper bound for the initial condition ϕ_0 in our numerical calculations.

where $\tilde{r}_{\max}^{\text{fixed}}$ must be chosen in such a way that the upper limits of integration in the numerical coordinates satisfy $r_{\text{conformal}} \leq r_{\max}^{\text{var}} = \sqrt{h_0^{\text{far}}} \left[\tilde{r}_{\max}^{\text{fixed}} - a_0^{\text{far}} + \ln \left(\phi^{1/\nu} \right) \right] \leq r_{\max}$ for all the geometries considered. We found that for $\tilde{r}_{\max}^{\text{fixed}} \sim 33$ such requirement is met. We also checked that one can vary the value of the ultraviolet cutoff $\tilde{r}_{\max}^{\text{fixed}}$ and the results for the holographic magnetic susceptibility do not change, which confirms the stability of our numerical procedure. We can now use (2.23) to describe the recent lattice data from [52] for the magnetic susceptibility of (2 + 1)-flavor QCD at zero magnetic field. A description of the lattice data can be obtained using

$$f(\phi) = 1.12 \operatorname{sech}(1.05 \phi - 1.45), \quad (2.24)$$

with the corresponding results displayed in Fig. 3. One can see that the holographic calculation provides a reasonable description of the lattice data in the temperature range we considered.

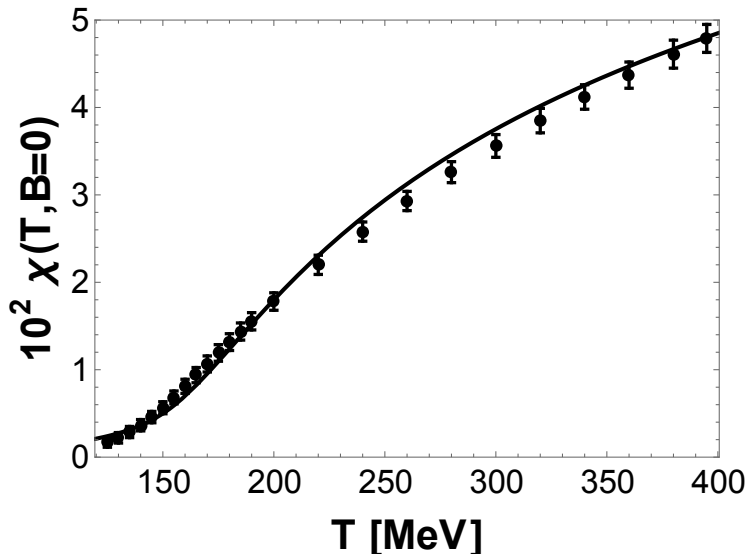


Figure 3: Holographic calculation of the magnetic susceptibility at zero magnetic field (solid line). The lattice data points are taken from [52] (we consider 10.9 times the data available in table III in [52], which corresponds to the magnetic susceptibility in natural units - see footnote 1 in [52]).

With the dilaton potential (2.19) and the Maxwell-Dilaton gauge coupling (2.24) fixed by the description of lattice data at zero magnetic field, our holographic model is now fully determined. This setup may be employed to investigate the physics of the dual quantum field theory at finite temperature and nonzero magnetic field as long as one keeps in mind the following limitations of the holographic model presented here:

- The model cannot describe phenomena directly related to chiral symmetry and its breaking/restoration (such as $T = 0$ magnetic catalysis [99–101]). This could be

studied by adding flavored Dp -branes in the bulk (see [80]);

- Clearly, the model cannot properly describe hadron thermodynamics (which sets in at low temperatures, below $T \sim 150$ MeV) and the effects of magnetic fields at low temperatures (for a study of the hadron resonance gas in a magnetic field see [98]). Moreover, in this holographic model asymptotic freedom is replaced by conformal invariance at sufficiently high temperatures. Therefore, this model is mostly useful (and perhaps realistic) to understand the effects of strong magnetic fields on the QGP at temperatures $T \sim 150 - 400$ MeV where pure hadronic physics and asymptotic freedom are not as relevant.

3 Holographic QCD thermodynamics at nonzero magnetic field

In this section the results for the holographic equation of state at nonzero magnetic field are presented. The formulas needed to compute the observables shown below were presented in the last section. Here, we define the pressure as the temperature integral of the entropy density performed while keeping the magnetic field fixed¹⁵

$$p(T, B) = \int_{T_{\text{ref}}}^T dT' s(T', B), \quad (3.1)$$

where we took a low reference temperature, $T_{\text{ref}} = 22$ MeV, in agreement with what was done in [61, 63] to obtain the fit for the dilaton potential and the gravitational constant (2.19). By doing so, the holographic curves for the pressure in Fig. 4 (and 2) actually correspond to the differences with respect to reference pressures calculated at T_{ref} for each value of the magnetic field. In Fig. 4 we show our holographic results for the normalized entropy density, s/T^3 , and pressure, p , and compare them to recent lattice data [53] for $eB = 0, 0.3, \text{ and } 0.6 \text{ GeV}^2$. It is important to remark, however, that the above convention to calculate the pressure is not exactly the same used in [53] since in (3.1) the pressure (difference) vanishes at $T = T_{\text{ref}} = 22$ MeV while in the calculation carried out in [53] the pressure goes like $\sim \mathcal{O}((eB)^4)$ for $T \rightarrow 0$ and, therefore, one should expect that the differences between these two calculations¹⁶ become more pronounced at low temperatures and large magnetic fields, as seen in Fig. 4. However, even for $eB = 0.6 \text{ GeV}^2$, we do find a reasonable agreement for the pressure at large temperatures ($T > 200$ MeV).

¹⁵As discussed in detail in Section 2 of [53] this corresponds to the isotropic pressure in the so-called “ B -scheme” where the magnetic field is kept fixed during compression. Also, this corresponds to the anisotropic pressure in the direction of the magnetic field in the so-called “ Φ -scheme” where the magnetic flux is kept fixed during compression.

¹⁶Note that in [53] the pressure was obtained from the renormalized free energy density. Here, we could have done the analogous holographic procedure by calculating the free energy density from the holographically renormalized on-shell action for the EMD model. This is, however, a much more laborious calculation than the one we have carried out here where we first calculated the entropy density using the Bekenstein-Hawking’s relation (2.18) and then we calculated the pressure (difference) using Eq. (3.1).

On the other hand, when it comes to the ratio s/T^3 , the agreement between our holographic results and the lattice is only at the qualitative level. This is in part due to the uncertainties in the holographic description of this observable already at $B = 0$: the holographic model parameters were chosen to describe the lattice data for the pressure and the speed of sound squared at $B = 0$ and not¹⁷ s/T^3 . In any case, one can see that s/T^3 increases with an increasing magnetic field, which is the general behavior observed on the lattice [53]. Moreover, note that the curve s/T^3 becomes steeper near the transition region for increasing values of the magnetic field, which is again in agreement with the general trend observed on the lattice [46].

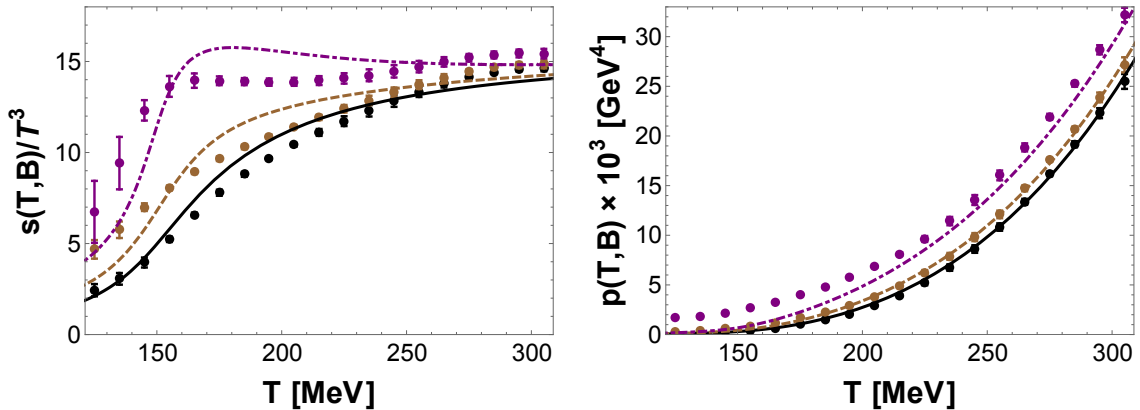


Figure 4: (Color online) Holographic calculation for the normalized entropy density, s/T^3 , and pressure, p , in the presence of an external magnetic field. The solid, dashed, and dot-dashed curves correspond to magnetic fields $eB = 0, 0.3, \text{ and } 0.6 \text{ GeV}^2$, respectively. The data points correspond to the lattice calculations for these quantities performed in [53].

As discussed in [53], the inflection point of s/T^3 may be used to characterize the crossover temperature as a function of the magnetic field¹⁸. Correspondingly, the peak in $T\partial_T(s/T^3)$ may be used to estimate the crossover temperature as a function of the magnetic field in our holographic model. We used our results for s/T^3 to find how the crossover temperature changes with a magnetic field and the results are displayed in table 1 and in Fig. 5. One can see in Fig. 5 that in our model the crossover temperature decreases with

¹⁷We believe that a better agreement with the lattice data at nonzero B may be obtained by improving the choice of the parameters of the holographic model by performing a global fit to the lattice data for the pressure, the entropy density, the speed of sound squared, and the trace anomaly at $B = 0$. We postpone this analysis for a future work.

¹⁸Since the crossover transition is not a genuine phase transition, the free energy is analytic in the temperature region where the degrees of freedom of the system change from a hadron gas to a deconfined plasma. Thus, the definition of the deconfinement temperature depends on the observable one uses to characterize it. Some possible options (which do not directly involve the chiral condensate) are, for instance, the minimum of the speed of sound squared, the peak of the normalized trace anomaly, and also the inflection point of the normalized entropy density. Each of them can give in principle a different value for the crossover temperature and one may use these different values to obtain a range of temperatures that defines the crossover region [17, 53].

an increasing magnetic field, as found on the lattice [17, 53], but a quantitative agreement with the data from [53] occurs only for $eB < 0.3 \text{ GeV}^2$.

$eB \text{ [GeV}^2\text{]}$	$T_c(eB) \text{ [MeV]}$
0	158.2
0.1	157.6
0.2	154.9
0.3	153.2
0.4	151.3
0.5	149.9

Table 1: Deconfinement temperature (defined by the inflection point of s/T^3) for different values of the magnetic field in the bottom-up holographic model.

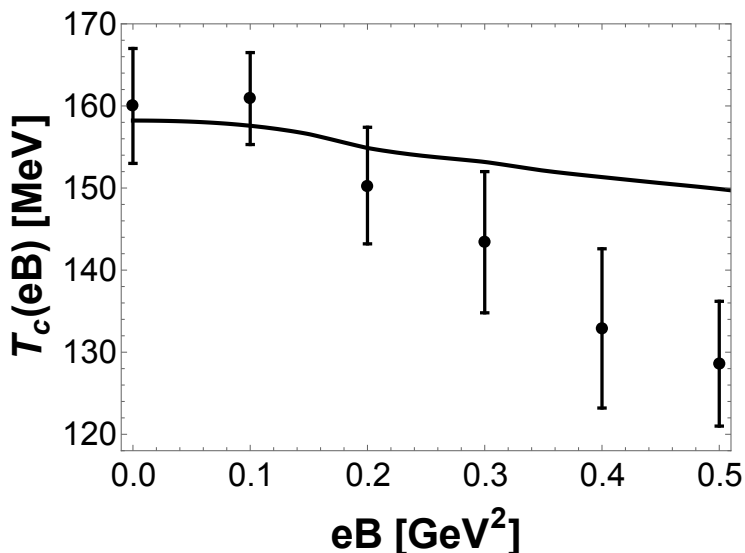


Figure 5: Deconfinement temperature (defined by the inflection point of s/T^3) for different values of the magnetic field in the bottom-up holographic model. The data points correspond to the lattice calculation performed in [53].

As a technical detail, in order to obtain the curves in Fig. 4 we used a large grid of initial conditions with 720000 points taking 900 equally spaced points in the ϕ_0 -direction starting from $\phi_0 = 0.3$ and going up to $\phi_0 = 7.8$, and 800 equally spaced points in the $\frac{\mathcal{B}}{\mathcal{B}_{\max}(\phi_0)}$ -direction starting from $\frac{\mathcal{B}}{\mathcal{B}_{\max}(\phi_0)} = 0$ and going up to $\frac{\mathcal{B}}{\mathcal{B}_{\max}(\phi_0)} = 0.99$. A large number of points was required to obtain sufficiently smooth curves for s/T^3 that allowed for the extraction of the crossover temperature and its dependence on the magnetic field. However, smooth curves for p could be obtained using much smaller (and faster) grids.

4 Concluding remarks and perspectives

In this paper we developed a bottom-up holographic model that provides a description of the crossover behavior observed in the equation of state and in the magnetic susceptibility of a QCD plasma with $(2+1)$ -flavors at zero magnetic field. We employed this model to study how an Abelian magnetic field B affects the thermodynamic properties of this strongly coupled plasma. In the presence of the magnetic field the plasma becomes anisotropic and we used the inflection point of the holographically determined s/T^3 curve to determine how the crossover temperature is affected by the external magnetic field. We found that the crossover temperature decreases with an increasing magnetic field, which agrees with the general behavior recently observed on the lattice. Our model calculations are in general quantitative agreement with the lattice data for moderately large values of the magnetic field up to $eB < 0.3 \text{ GeV}^2$. As far as we know, the holographic setup studied here is the only model that is able to achieve quantitative agreement with recent lattice calculations near the crossover transition for $0 < eB < 0.3 \text{ GeV}^2$, which is the expected range of magnetic field values achieved in ultrarelativistic heavy ion collisions. We believe that this agreement with the lattice data can be further improved towards larger values of eB if one tries to carefully match the lattice thermodynamic calculations at $B = 0$ by simultaneously taking into account different observables such as the pressure and the speed of sound squared, as we have done in the present approach, with the addition of the entropy density and the trace anomaly in a global fit; in this sense, our choice for the holographic model parameters at $B = 0$ may be systematically improved.

An interesting feature of our holographic model that distinguishes it from other constructions (such as [102, 103]) is that the suppression of the crossover temperature with the external field found here is directly tied to a *quantitative description* of near crossover lattice QCD thermodynamics at $B = 0$. Moreover, since in our model direct effects related to chiral symmetry are not taken into account, the fact that we find that the crossover temperature decreases with B (and that we do observe some level of quantitative agreement with lattice data) may give support to the idea that the inverse magnetic catalysis observed on the lattice [17] is less related to the chiral condensate than to an adequate description of deconfinement, as suggested in [104, 105]. Moreover, motivated by the recent studies in Refs. [106] and [46], one could also investigate if the present holographic model indicates the existence of a critical point in the (T, B) -plane.

The holographic setup constructed here may be employed to obtain estimates for the magnetic field dependence of many other properties of the QGP. For instance, our non-conformal model can be used to investigate the interplay between a dynamically generated infrared scale and the external magnetic field in the study of nonequilibrium phenomena. For instance, one could generalize the calculation of transport coefficients performed in [69] and obtain a quantitative estimate of how the shear (and bulk) viscosity coefficients vary with the external field near the QCD crossover transition.

Recently, the effects of an external magnetic field on the equilibration dynamics of

strongly coupled plasmas have been studied using holography [71, 107]. In this context, it would be interesting to see how the quasinormal mode spectrum in our nonconformal plasma varies with an external magnetic field. Given that our model can capture the nonconformal behavior of the QGP near the crossover transition (with and without the external magnetic field), a detailed study of the quasinormal modes in this model may shed some light on the thermalization process that takes place in an anisotropic (nonconformal) strongly magnetized QGP. We hope to report results in this direction in the near future.

Acknowledgments

We thank I. A. Shovkovy and E. S. Fraga for discussions about the effects of magnetic fields on the QGP and F. Bruckmann and G. Endrodi for comments on the manuscript. We also thank the authors of Ref. [53] for making their lattice results available to us. J. N. thanks the Columbia University Physics Department for its hospitality. This work was supported by Fundação de Amparo à Pesquisa do Estado de São Paulo (FAPESP) and Conselho Nacional de Desenvolvimento Científico e Tecnológico (CNPq).

References

- [1] BRAHMS collaboration, I. Arsene et al., Nucl. Phys. A **757**, 1 (2005), [arXiv:nucl-ex/0410020].
- [2] PHENIX collaboration, K. Adcox et al., Nucl. Phys. A **757**, 184 (2005), [arXiv:nucl-ex/0410003].
- [3] PHOBOS collaboration, B. B. Back et al., Nucl. Phys. A **757**, 28 (2005), [arXiv:nucl-ex/0410022].
- [4] STAR collaboration, J. Adams et al., Nucl. Phys. A **757**, 102 (2005), [arXiv:nucl-ex/0501009].
- [5] M. Gyulassy and L. McLerran, Nucl. Phys. A **750**, 30 (2005), [arXiv:nucl-th/0405013].
- [6] U. Heinz and R. Snellings, Ann. Rev. Nucl. Part. Sci. **63**, 123 (2013), [arXiv:1301.2826 [nucl-th]].
- [7] E. Shuryak, [arXiv:1412.8393 [hep-ph]].
- [8] D. E. Kharzeev, L. D. McLerran and H. J. Warringa, Nucl. Phys. A **803**, 227 (2008), [arXiv:0711.0950 [hep-ph]].
- [9] K. Fukushima, D. E. Kharzeev and H. J. Warringa, Phys. Rev. D **78**, 074033 (2008), [arXiv:0808.3382 [hep-ph]].
- [10] V. Skokov, A. Y. Illarionov and V. Toneev, Int. J. Mod. Phys. A **24**, 5925 (2009), [arXiv:0907.1396 [nucl-th]].
- [11] K. Tuchin, Adv. High Energy Phys. **2013**, 490495 (2013), [arXiv:1301.0099 [hep-ph]].
- [12] W. -T. Deng and X. -G. Huang, Phys. Rev. C **85**, 044907 (2012), arXiv:1201.5108 [nucl-th]].

- [13] J. Bloczynski, X. -G. Huang, X. Zhang and J. Liao, Phys. Lett. B **718**, 1529 (2013), [arXiv:1209.6594 [nucl-th]].
- [14] U. Gursoy, D. Kharzeev and K. Rajagopal, Phys. Rev. C **89**, no. 5, 054905 (2014) [arXiv:1401.3805 [hep-ph]].
- [15] T. Vachaspati, Phys. Lett. B **265**, 258 (1991).
- [16] D. Grasso and H. R. Rubinstein, Phys. Rept. **348**, 163 (2001), [arXiv:astro-ph/0009061].
- [17] G. S. Bali, F. Bruckmann, G. Endrodi, Z. Fodor, S. D. Katz, S. Krieg, A. Schafer and K. K. Szabo, JHEP **02** (2012) 044, [arXiv:1111.4956 [hep-lat]].
- [18] R. C. Duncan and C. Thompson, Astrophys. J. **392**, L9 (1992).
- [19] N. O. Agasian and S. M. Fedorov, Phys. Lett. B **663**, 445 (2008) [arXiv:0803.3156 [hep-ph]].
- [20] A. J. Mizher, M. N. Chernodub and E. S. Fraga, Phys. Rev. D **82**, 105016 (2010) [arXiv:1004.2712 [hep-ph]].
- [21] N. Evans, T. Kalaydzhyan, K. Y. Kim and I. Kirsch, JHEP **1101**, 050 (2011) [arXiv:1011.2519 [hep-th]].
- [22] F. Preis, A. Rebhan and A. Schmitt, JHEP **1103**, 033 (2011) [arXiv:1012.4785 [hep-th]].
- [23] K. Fukushima and J. M. Pawłowski, Phys. Rev. D **86**, 076013 (2012) [arXiv:1203.4330 [hep-ph]].
- [24] G. S. Bali, F. Bruckmann, G. Endrodi, Z. Fodor, S. D. Katz and A. Schafer, Phys. Rev. D **86**, 071502 (2012) [arXiv:1206.4205 [hep-lat]].
- [25] K. Fukushima and Y. Hidaka, Phys. Rev. Lett. **110**, no. 3, 031601 (2013) [arXiv:1209.1319 [hep-ph]].
- [26] J. P. Blaizot, E. S. Fraga and L. F. Palhares, Phys. Lett. B **722**, 167 (2013) [arXiv:1211.6412 [hep-ph]].
- [27] N. Callebaut and D. Dudal, Phys. Rev. D **87**, no. 10, 106002 (2013) [arXiv:1303.5674 [hep-th]].
- [28] G. S. Bali, F. Bruckmann, G. Endrodi, F. Gruber and A. Schaefer, JHEP **1304**, 130 (2013) [arXiv:1303.1328 [hep-lat]].
- [29] C. Bonati, M. D'Elia, M. Mariti, M. Mesiti, F. Negro and F. Sanfilippo, Phys. Rev. D **89**, no. 11, 114502 (2014) [arXiv:1403.6094 [hep-lat]].
- [30] K. Fukushima and P. Morales, Phys. Rev. Lett. **111**, 051601 (2013) [arXiv:1305.4115 [hep-ph]].
- [31] C. S. Machado, F. S. Navarra, E. G. de Oliveira, J. Noronha and M. Strickland, Phys. Rev. D **88**, 034009 (2013) [arXiv:1305.3308 [hep-ph]].
- [32] E. S. Fraga, B. W. Mintz and J. Schaffner-Bielich, Phys. Lett. B **731**, 154 (2014) [arXiv:1311.3964 [hep-ph]].
- [33] J. O. Andersen, W. R. Naylor and A. Tranberg, JHEP **1404**, 187 (2014) [arXiv:1311.2093 [hep-ph]].
- [34] G. S. Bali, F. Bruckmann, G. Endrodi and A. Schafer, Phys. Rev. Lett. **112**, 042301 (2014) [arXiv:1311.2559 [hep-lat]].

- [35] M. Ferreira, P. Costa and C. Providência, *Phys. Rev. D* **89**, no. 3, 036006 (2014) [arXiv:1312.6733 [hep-ph]].
- [36] M. Ruggieri, L. Oliva, P. Castorina, R. Gatto and V. Greco, *Phys. Lett. B* **734**, 255 (2014) [arXiv:1402.0737 [hep-ph]].
- [37] M. Ferreira, P. Costa, O. Lourenço, T. Frederico and C. Providência, *Phys. Rev. D* **89**, no. 11, 116011 (2014) [arXiv:1404.5577 [hep-ph]].
- [38] R. L. S. Farias, K. P. Gomes, G. I. Krein and M. B. Pinto, *Phys. Rev. C* **90**, no. 2, 025203 (2014) [arXiv:1404.3931 [hep-ph]].
- [39] A. Ayala, M. Loewe, A. J. Mizher and R. Zamora, *Phys. Rev. D* **90**, no. 3, 036001 (2014) [arXiv:1406.3885 [hep-ph]].
- [40] A. Ayala, M. Loewe and R. Zamora, *Phys. Rev. D* **91**, no. 1, 016002 (2015) [arXiv:1406.7408 [hep-ph]].
- [41] E. J. Ferrer, V. de la Incera and X. J. Wen, *Phys. Rev. D* **91**, no. 5, 054006 (2015) [arXiv:1407.3503 [nucl-th]].
- [42] K. Kamikado and T. Kanazawa, *JHEP* **1501**, 129 (2015) [arXiv:1410.6253 [hep-ph]].
- [43] L. Yu, J. Van Doorselaere and M. Huang, *Phys. Rev. D* **91**, no. 7, 074011 (2015) [arXiv:1411.7552 [hep-ph]].
- [44] J. Braun, W. A. Mian and S. Rechenberger, arXiv:1412.6025 [hep-ph].
- [45] N. Mueller and J. M. Pawłowski, arXiv:1502.08011 [hep-ph].
- [46] G. Endrodi, arXiv:1504.08280 [hep-lat].
- [47] E. S. Fraga, *Lect. Notes Phys.* **871**, 121 (2013) [arXiv:1208.0917 [hep-ph]].
- [48] D. Kharzeev, K. Landsteiner, A. Schmitt and H. -U. Yee, *Lect. Notes Phys.* **871**, 1 (2013).
- [49] J. O. Andersen, W. R. Naylor and A. Tranberg, [arXiv:1411.7176 [hep-ph]].
- [50] V. A. Miransky and I. A. Shovkovy, *Phys. Rept.* **576**, 1 (2015) [arXiv:1503.00732 [hep-ph]].
- [51] Z. Fodor and S. D. Katz, [arXiv:0908.3341 [hep-ph]].
- [52] C. Bonati, M. D'Elia, M. Mariti, F. Negro and F. Sanfilippo, *Phys. Rev. D* **89**, 054506 (2014), [arXiv:1310.8656 [hep-lat]].
- [53] G. S. Bali, F. Bruckmann, G. Endrodi, S. D. Katz and A. Schafer, *JHEP* **08** (2014) 177, [arXiv:1406.0269 [hep-lat]].
- [54] J. Maldacena, *Adv. Theor. Math. Phys.* **2**, 231 (1998), [arXiv:hep-th/9711200].
- [55] S. S. Gubser, I. R. Klebanov and A. M. Polyakov, *Phys. Lett. B* **428**, 105 (1998), [arXiv:hep-th/9802109].
- [56] E. Witten, *Adv. Theor. Math. Phys.* **2**, 253 (1998), [arXiv:hep-th/9802150].
- [57] J. Casalderrey-Solana, H. Liu, D. Mateos, K. Rajagopal and U. A. Wiedemann, [arXiv:1101.0618 [hep-th]].
- [58] A. Adams, L. D. Carr, T. Schaefer, P. Steinberg and J. E. Thomas, *New J. Phys.* **14**, 115009 (2012), [arXiv:1205.5180 [hep-th]].
- [59] S. S. Gubser, A. Nellore, S. S. Pufu and F. D. Rocha, *Phys. Rev. Lett.* **101**, 131601 (2008), [arXiv:0804.1950 [hep-th]].

- [60] S. I. Finazzo and J. Noronha, Phys. Rev. D **89**, 106008 (2014), [arXiv:1311.6675 [hep-th]].
- [61] S. I. Finazzo, R. Rougemont, H. Marrochio and J. Noronha, JHEP **02** (2015) 051, [arXiv:1412.2968 [hep-ph]].
- [62] O. DeWolfe, S. S. Gubser and C. Rosen, Phys. Rev. D **84**, 126014 (2011), [arXiv:1108.2029 [hep-th]].
- [63] R. Rougemont, S. I. Finazzo, A. Ficnar and J. Noronha, *Holographic QCD thermodynamics, energy loss, and thermalization at finite temperature and baryon chemical potential*, to appear.
- [64] H. B. Meyer, Eur. Phys. J. A **47**, 86 (2011) [arXiv:1104.3708 [hep-lat]].
- [65] E. D'Hoker and P. Kraus, JHEP **0910**, 088 (2009), [arXiv:0908.3875 [hep-th]].
- [66] E. D'Hoker and P. Kraus, Class. Quant. Grav. **27**, 215022 (2010), [arXiv:1006.2573 [hep-th]].
- [67] E. D'Hoker and P. Kraus, Lect. Notes Phys. **871**, 469 (2013), [arXiv:1208.1925 [hep-th]].
- [68] G. Basar, D. E. Kharzeev, Phys. Rev. D **85**, 086012 (2012), [arXiv:1202.2161 [hep-th]].
- [69] R. Critelli, S. I. Finazzo, M. Zaniboni and J. Noronha, Phys. Rev. D **90**, 066006 (2014), [arXiv:1406.6019 [hep-th]].
- [70] R. Rougemont, R. Critelli and J. Noronha, Phys. Rev. D **91**, 066001 (2015), [arXiv:1409.0556 [hep-th]].
- [71] J. F. Fuini III and L. G. Yaffe, [arXiv:1503.07148 [hep-th]].
- [72] Sz. Borsanyi, G. Endrodi, Z. Fodor, S. D. Katz, S. Krieg, C. Ratti and K. K. Szabo, JHEP **08** (2012) 053, [arXiv:1204.6710 [hep-lat]].
- [73] Y. Aoki, G. Endrodi, Z. Fodor, S. D. Katz and K. K. Szabo, Nature **443**, 675 (2006) [hep-lat/0611014].
- [74] S. S. Gubser and A. Nellore, Phys. Rev. D **78**, 086007 (2008), [arXiv:0804.0434 [hep-th]].
- [75] S. I. Finazzo and J. Noronha, Phys. Rev. D **90**, 115028 (2014), [arXiv:1411.4330 [hep-th]].
- [76] U. Gursoy, E. Kiritsis and F. Nitti, JHEP **02** (2008) 019, [arXiv:0707.1349 [hep-th]].
- [77] U. Gursoy and E. Kiritsis, JHEP **02** (2008) 032, [arXiv:0707.1324 [hep-th]].
- [78] U. Gursoy, E. Kiritsis, L. Mazzanti and F. Nitti, JHEP **05** (2009) 033, [arXiv:0812.0792 [hep-th]].
- [79] O. DeWolfe, S. S. Gubser and C. Rosen, Phys. Rev. D **83**, 086005 (2011), [arXiv:1012.1864 [hep-th]].
- [80] T. Alho, M. Jarvinen, K. Kajantie, E. Kiritsis, C. Rosen and K. Tuominen, JHEP **04** (2014) 124, [arXiv:1312.5199 [hep-ph]].
- [81] G. Veneziano, Nucl. Phys. B **117**, 519 (1976).
- [82] J. Noronha, Phys. Rev. D **81**, 045011 (2010) [arXiv:0910.1261 [hep-th]].
- [83] J. Noronha, Phys. Rev. D **82**, 065016 (2010) [arXiv:1003.0914 [hep-th]].
- [84] A. Ficnar, J. Noronha and M. Gyulassy, Nucl. Phys. A **855**, 372 (2011) [arXiv:1012.0116 [hep-ph]].
- [85] A. Ficnar, J. Noronha and M. Gyulassy, J. Phys. G **38**, 124176 (2011) [arXiv:1106.6303 [hep-ph]].

- [86] A. Ficnar, J. Noronha and M. Gyulassy, Nucl. Phys. A **910-911**, 252 (2013) [arXiv:1208.0305 [hep-ph]].
- [87] R. A. Janik, G. Plewa, H. Soltanpanahi and M. Spalinski, arXiv:1503.07149 [hep-th].
- [88] J. W. York Jr., Phys. Rev. Lett. **28**, 1082 (1972).
- [89] G. W. Gibbons and S. W. Hawking, Phys. Rev. D **15**, 2752 (1977).
- [90] M. Henningson and K. Skenderis, JHEP **07** (1998) 023, [arXiv:hep-th/9806087].
- [91] S. de Haro, K. Skenderis and S. N. Solodukhin, Commun. Math. Phys. **217**, 595 (2001), [arXiv:hep-th/0002230].
- [92] K. Skenderis, Class. Quant. Grav. **19**, 5849 (2002), [arXiv:hep-th/0209067].
- [93] I. Papadimitriou, JHEP **08** (2011) 119, [arXiv:1106.4826 [hep-th]].
- [94] J. Lindgren, I. Papadimitriou, A. Taliotis and J. Vanhoof, [arXiv:1505.04131 [hep-th]].
- [95] J. D. Bekenstein, Phys. Rev. D **7**, 2333 (1973).
- [96] S. W. Hawking, Commun. Math. Phys. **43**, 199 (1975); [Erratum-ibid. **46**, 206 (1976)].
- [97] M. Blake, A. Donos and N. Lohitsiri, [arXiv:1502.03789 [hep-th]].
- [98] G. Endrödi, JHEP **1304**, 023 (2013) [arXiv:1301.1307 [hep-ph]].
- [99] V. P. Gusynin, V. A. Miransky and I. A. Shovkovy, Phys. Rev. Lett. **73**, 3499 (1994) [Phys. Rev. Lett. **76**, 1005 (1996)] [hep-ph/9405262].
- [100] V. P. Gusynin, V. A. Miransky and I. A. Shovkovy, Nucl. Phys. B **462**, 249 (1996) [hep-ph/9509320].
- [101] V. A. Miransky and I. A. Shovkovy, Phys. Rev. D **66**, 045006 (2002) [hep-ph/0205348].
- [102] A. Ballon-Bayona, JHEP **1311**, 168 (2013) [arXiv:1307.6498 [hep-th]].
- [103] K. A. Mamo, JHEP **1505**, 121 (2015) [arXiv:1501.03262 [hep-th]].
- [104] E. S. Fraga and L. F. Palhares, Phys. Rev. D **86**, 016008 (2012) [arXiv:1201.5881 [hep-ph]].
- [105] E. S. Fraga, J. Noronha and L. F. Palhares, Phys. Rev. D **87**, no. 11, 114014 (2013) [arXiv:1207.7094 [hep-ph]].
- [106] T. D. Cohen and N. Yamamoto, Phys. Rev. D **89**, 054029 (2014), [arXiv:1310.2234 [hep-ph]].
- [107] K. A. Mamo and H. U. Yee, arXiv:1505.01183 [hep-ph].